Properties of squeeze cast Mg-6Zn-3Cu alloy and its saffil alumina short fibre reinforced composites

S. JAYALAKSHMI, SATISH V. KAILAS, S. SESHAN
Department of Mechanical Engineering, Indian Institute of Science, Bangalore 560 012, India

E. FLEURY*
Advanced Materials Research Center, Materials Science Division, Korea Institute of Science & Technology (KIST), Seoul 130 650, Korea
E-mail: efleury@kist.re.kr

Published online: 10 April 2006

In the present work, Mg-Zn-Cu alloy (ZC63) and its saffil alumina short fibre reinforced composites produced using the squeeze casting technique were evaluated for their properties. The unreinforced base alloys and their composites were characterized for their microstructure, hardness, yield strength, impact strength, wear resistance and corrosion resistance. The dependence of the properties of composites was studied as a function of fibre volume fraction. Results showed that the composites exhibited improved hardness, yield strength at elevated temperature and wear resistance in comparison to the monolithic alloy. However, ductility, impact strength and corrosion resistance of the composites were inferior to that of the base alloy. The nature of the base alloy matrix in determining the properties of the composites was discussed based on fractographic analysis.

1. Introduction

Magnesium alloy castings have attained a prominent position in the transport industry mainly due to their high strength-to-weight ratio [1]. However, many of the magnesium cast alloys have limited ductility and exhibit low strength at elevated temperature that restrict their use [2, 3]. Over the past two decades, extensive research on alloying of magnesium has paved way for new Mg alloy systems such as the Mg-Zn system. Among these, the Mg-Zn-Cu alloys exhibit relatively high ductility and high strength [2, 4]. In these alloys, the addition of Cu and Zn imparts grain-refining effect, and improves castability and ductility [4]. These alloys are considered as possible replacement materials in automobile engine castings such as in cylinder blocks and sumps [5]. In addition to strength properties, applications involving magnesium alloys also require appreciable thermal stability, specific stiffness, wear resistance and corrosion resistance [6]. Addition of ceramic reinforcements to the base alloys to produce metal matrix composites (MMCs), has proved to be an answer to improve some of these properties in many non-ferrous systems [6–8]. Neih *et al.* [6] and Fukunaga *et al.* [8] have reported significant improvement in hardness, elastic modulus, strength and wear resistance in discontinuously reinforced aluminium matrix composites, whereas Hasson *et al.* [7] reported decrease in ductility and impact resistance. Though data available on magnesium MMCs is meager, the available literature [9–12] is indicative of its large potential as a promising material in many aerospace, railway transport and automotive applications.

In the work reported here, the ZC63 magnesium alloy and its saffil alumina short fibre reinforced composites were produced by the squeeze casting and squeeze infiltration methods respectively. As the magnesium metal is difficult to handle in the molten state [12], the process parameters during melting and casting were optimized systematically to achieve sound castings of both the alloy and its composites. The resulting castings were analyzed for their microstructure, mechanical properties, wear resistance and corrosion resistance. The effect of fibre reinforcement and the importance of the base alloy matrix in determining the behaviour were further examined.

2. Experimental details

Magnesium alloy ZC63 (Mg-5.5 to 6.5 Zn-2.5 to 3.5 Cu and 0.25 to 0.75 Mn, expressed in wt%) and its

*Author to whom all correspondence should be addressed.
0022-2461
DOI: 10.1007/s10853-005-4484-0

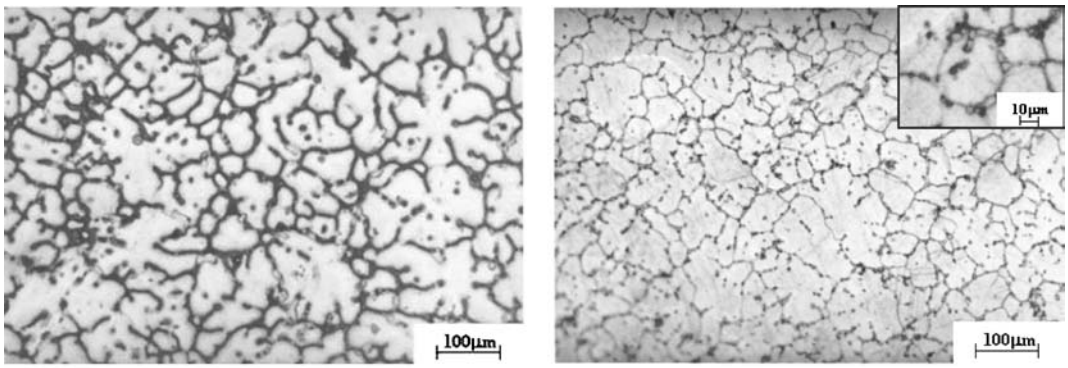

Figure 1 Optical micrographs of unreinforced ZC63 alloy (a) as-cast condition (b) heat-treated condition (inset shows spherodized eutectic at grain boundaries, formed due to heat treatment.

composites were produced using the squeeze casting and squeeze infiltration methods respectively. Saffil® alumina short fibres were used as the reinforcement material (mean fibre diameter: 3μ mm and fibre length: 200μ mm). Three volume fractions (viz., 15, 20 and 25%) of fibre preforms with diameter: 70 mm and height: 35 mm were used. Magnesium was melted using the fluxless process [13] in a reducing atmosphere to prevent oxidation of the molten metal. For the composites, the preform was pre-heated to a temperature of 850°C for all volume fractions. Both the alloy and its composites were produced at a squeeze pressure of 40 MPa. The aging cycle of the alloy and its composites (T6 condition [14]) were optimized to attain peak hardness. The aging treatment was done at a temperature of 190–210°C [14]. The hardness of the unreinforced alloy ZC63 and its composites was measured using a Brinell hardness tester with a 5 mm-ball indentor at 500 kg load. Tests were conducted on five specimens to ensure repeatability of peak hardness values. Microstructures were studied using optical and scanning electron microscopes. The alloy and composites in their peak-hardened condition were evaluated for their properties in the present study. Density and room temperature elastic modulus were determined using the specific-gravity method and non-destructive elastosonic method respectively. Tensile tests of the alloy and its composites were carried out in a 2-ton Monsanto tensometer provided with a high temperature furnace for testing at elevated temperatures. Tensile tests were conducted at temperatures of 25, 100, 150 and 200°C respectively, at a controlled strain rate of 0.001/s. Instrumented Charpy impact tests were conducted on bars of dimension $55\times10\times10$ mm^3, and on notched bars with notch root tip radius 0.02 mm. Dry sliding wear tests were conducted using cylindrical specimens of diameter 6 mm and height 15 mm, on a pin-on-disc machine with (a) EN24 steel disc and (b) SiC abrasive disc as the counterface materials. The sliding speed and normal load (stress) were kept constant at 1.5 m/sec and 30 N (~1 MPa) respectively. Corrosion tests were carried out in a salt-spray atmosphere for varying exposure period [15]. The specimens were cleaned after the tests to remove the corroded products. The corrosion rates were calculated based on the weight loss of the corroded specimens [15]. The surfaces of the specimens tested at different conditions, viz., tensile, impact, wear and corrosion, were analyzed using optical, stereo and scanning electron microscopes.

3. Results and discussion

3.1. Microstructure and aging response

Fig. 1a and b show the microstructures of the unreinforced ZC63 base alloy in the as-cast and heat-treated condition. The microstructure of the as-cast Mg-Zn-Cu alloy consists of a-Mg matrix and $Mg(Zn,Cu)_2$ eutectic compound that is present along the grain boundaries. The eutectic phase was identified as Laves phase by various authors [16–21]. Upon solution treatment and aging, $MgZn_2$ precipitates are formed and are distributed homogenously through out the matrix [12, 14, 16]. Fig. 1b shows that the grain boundary eutectic has become spherodized on aging (see inset), but however the precipitates could not be observed. Nunez-Lopez *et al.* [16] have reported that the eutectic phase gets partially spherodized during heat-treatment and that the precipitates formed during aging were unresolvable even at higher magnifications in SEM. Transmission electron microscopy was used by Yang *et al.* [19] and Yuan *et al.* [21] to resolve the $MgZn_2$ precipitates that formed during aging. Fig. 2a shows the representative microstructure of a 20%V_f composite that indicates uniform and homogeneous dispersion of fibres with no significant trace of porosity. The fibres are distributed in a planar random orientation due to the method of preparation of the preform [22]. The sufficiently higher temperature of the preform (850°C) than the molten metal (~800°C) enabled complete infiltration of the molten metal into the preform that prevented premature solidification of the metal. The absence of fibre clustering (Fig. 2a) indicates that the application of squeeze pressure has not compressed the preforms. Fig. 2a also shows protruded ends of fibres, which appear as small white globular regions. During polishing,

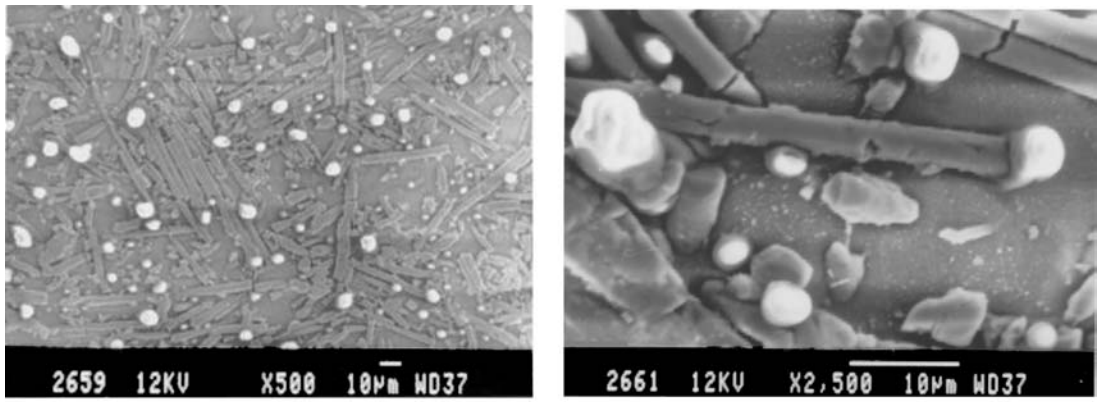

(a) (b)

Figure 2 SEM micrographs of (a) 20%V_f composite (b) fibre protrusions observed at high magnification.

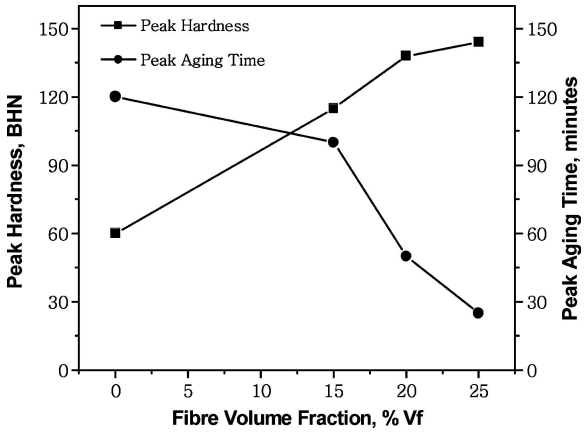

Figure 3 Variation of peak hardness and peak aging time with fibre volume fraction.

the ductile alloy matrix gets easily removed, thereby revealing the protruded fibre ends on the surface. Fig. 2b is a high magnification micrograph that shows fibre protrusions. Fig. 3 shows the peak hardness and peak aging time of the unreinforced alloy and its composites as a function of fibre volume fraction. From this figure it can be observed that the composites exhibit higher hardness than that of the unreinforced alloy, and that their hardness increases with increase in fibre volume fraction. In the composites, the increase in hardness is mainly due to the inherent load carrying capacity of the fibres [23]. In addition, the presence of Mg $(Zn,Cu)_2$ at the fibre/matrix interface leads to increased precipitation on aging [16], resulting at an overall increase in peak hardness with fibre volume fraction. It can also be observed that the peak aging time decreases with increase in fibre volume fraction. In the case of composites, the addition of fibres provides high dislocation density at the fibre/matrix interface that acts as heterogeneous nucleation sites for precipitation to occur, thereby accelerating the aging kinetics [24, 25]. This leads to the reduction in aging time with increase in the fibre volume fraction.

3.2. Density and elastic modulus

The density values of the unreinforced ZC63 base alloy and its composites measured by specific gravity method and that calculated using rule-of-mixtures (ROM) equation [26] are listed in Table I. The experimental values are obtained from the average of three measurements. Since the density of the reinforcement (alumina fibres: 3.3 g/cc) is greater than that of the base alloy (1.85 g/cc), the increase in fibre volume fraction linearly increases the density of the composites. It could also be observed that the experimental density values are comparable to those calculated theoretically using ROM equation. This further indicates that the presence of porosities is negligible and that the squeeze pressure applied was sufficient enough for complete infiltration and solidification of the molten metal.

Fig. 4 shows the experimentally determined elastic modulus as a function of fibre volume fraction, and those estimated using (i) Halpin-Tsai-Kardos type expression for discontinuous reinforcements [26] and (ii) ROM equations for fibres loaded along the longitudinal and transverse axis [26]. The measured values show that the elastic modulus increases with fibre volume fraction. Further, even at the lowest volume fraction of 15%V_f, an increase in the modulus by almost 70% with respect to the alloy is observed, which is due to the high inherent stiffness (300 GPa) of the ceramic reinforcements. It should be noted that the experimental values are comparable with those calculated using Halpin-Tsai-Kardos type expression for discontinuous reinforcements [26]. The experimental val-

TABLE I Experimental and calculated values of density of ZC63 base alloy and its composites.

Fibre volume fraction	Density, g/cc(avg. of 3 tests)(Experimental)	Density, g/cc (Calculated using ROM equations [26])
ZC63 Base Alloy	1.85	–
ZC63 + 15%V_f	2.12	2.06
ZC63 + 20%V_f	2.23	2.14
ZC63 + 25%V_f	2.30	2.21

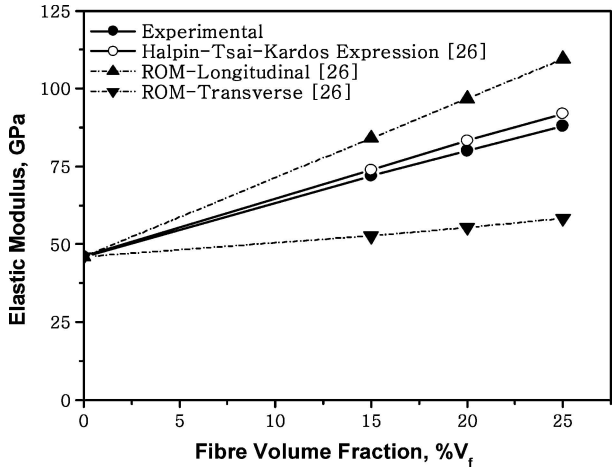

Figure 4 Variation of experimental and calculated values of elastic modulus with fibre volume fraction.

ues are also typical of discontinuous reinforcements [26] falling well within the upper and lower bound modulus values obtained using the respective ROM equations.

3.3. Tensile properties

Fig. 5a shows the yield strength of the alloy and composites as a function of test temperature. It can be observed that at room temperature, the strength of the composites is almost the same as that of the unreinforced alloy, the exception being 15%V_f that shows strength lesser than that of the alloy. With increase in test temperature, the unreinforced base alloy shows a drastic decrease in strength, such that, at the highest test temperature (200°C), the strength decreases to about one third of its room temperature value. Amongst the composites, the composite with 15%V_f shows improved strength at 100°C than that observed at room temperature, whereas retention in strength is observed for 20 and 25% composites at 100°C. Beyond 100°C, the composites of all volume fractions show a gradual reduction in strength with temperature. However, when compared to the alloy, they exhibit significant improvement in strength indicating the influence of fibre addition in improving the properties at higher temperatures. Fig. 5b shows the variation of %elongation of unreinforced alloy and its composites as a function of temperature. At higher test temperatures the alloy exhibits higher ductility when compared to that at room temperature. The lowering of %elongation at temperatures greater than 100°C is possibly due to the onset of over-aging that could occur at these temperatures. The composites exhibit low %elongation values in comparison to the unreinforced alloy at all test temperatures, which is due to the presence of brittle ceramic fibres. It can be observed that the unreinforced base alloy exhibits elongation value that is almost an order of magnitude greater than that of the composites. Fractographic analysis of the alloy at all test temperatures showed dominant ductile failure. Fig. 6a and b show the fracture surfaces of the alloy observed at room temperature and 150°C respectively.

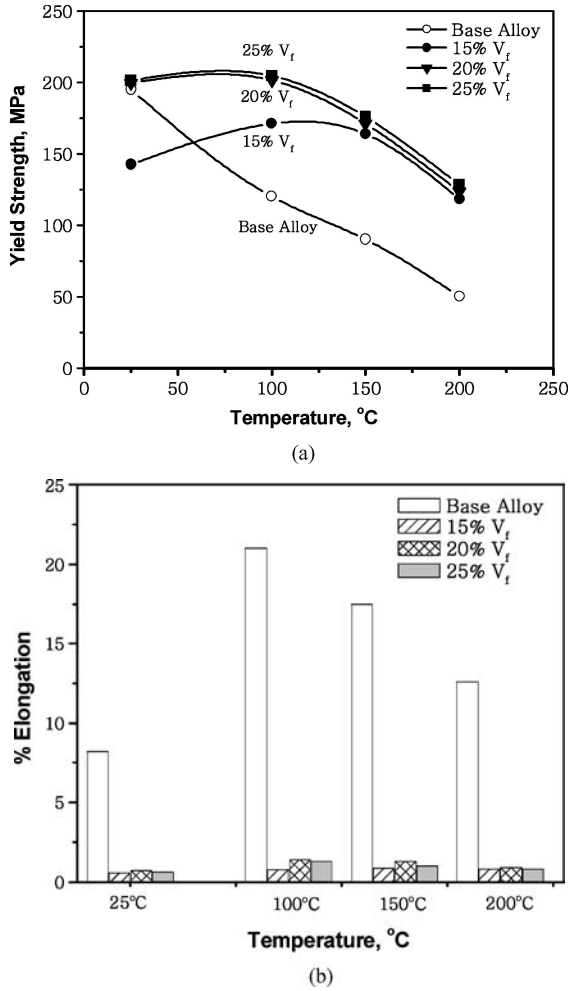

Figure 5 Variation of (a) yield strength of ZC63 alloy and its composites at different test temperatures and (b) % elongation of ZC63 alloy and its composites at different test temperatures.

Composites are usually considered advantageous over the base alloys for the reason that they provide improved strength at both room and elevated temperatures. Various authors [10, 22, 27] have reported significant improvement in room temperature strength in several Al- and Mg-based MMCs. However, in the present case, it can be observed from Fig. 5a that 15%V_f shows strength that is significantly lower than that of the alloy at room temperature, and that the composites with 20%V_f and 25%V_f do not exhibit any considerable improvement in strength over that of the unreinforced alloy.

Several authors have reported similar behaviour, where the room temperature strength of the composites was lower than that of the base alloy, and have attributed to various factors such as the properties of the alloy matrix, critical fibre volume fraction and residual stresses [22, 27–32]. A similar trend was observed by Friend [28, 31] in Al-MMCs with different alloy matrices. He observed that a critical volume fraction (V_{crit}) should be exceeded for significant strength improvement at room temperature and that the composites with fibre volume fraction less than V_{crit} exhibited strength much lower than that of the unreinforced alloy. Further, he suggested that the value of

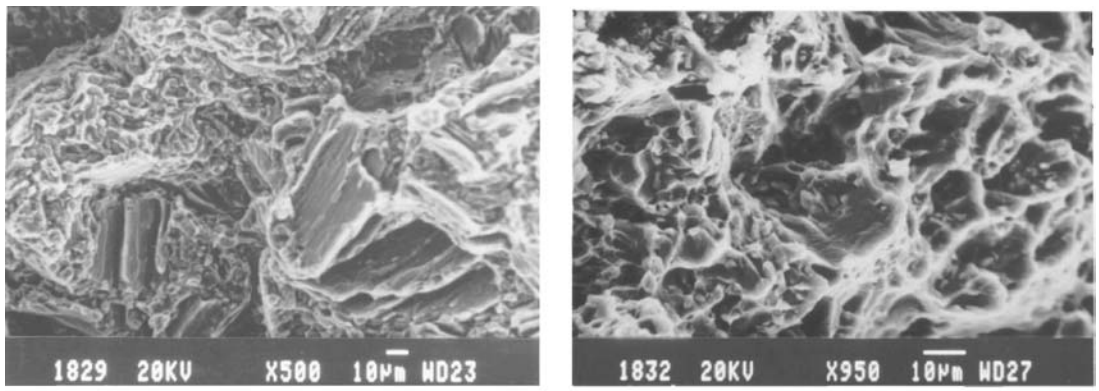

(a) (b)

Figure 6 Fractographic evidences showing dominant ductile failure of ZC63 alloy at (a) room temperature and (b) 150°C.

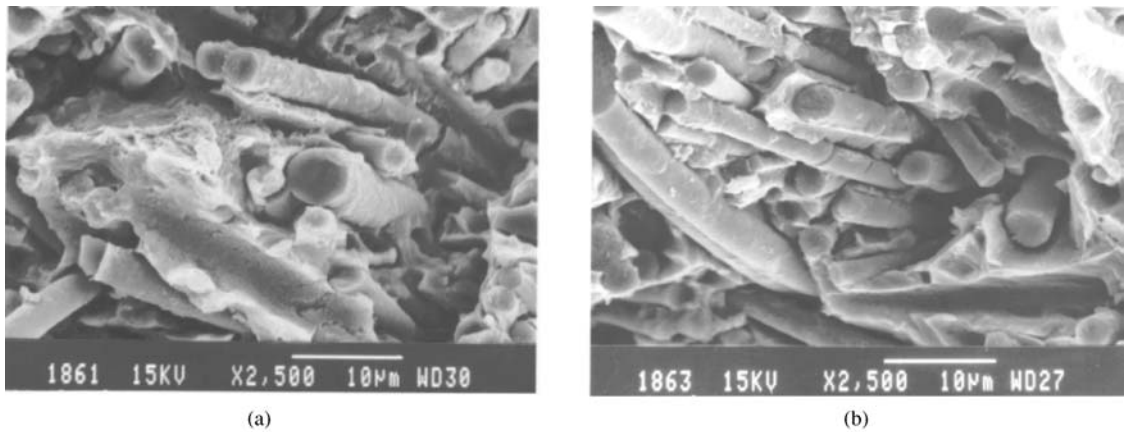

(a) (b)

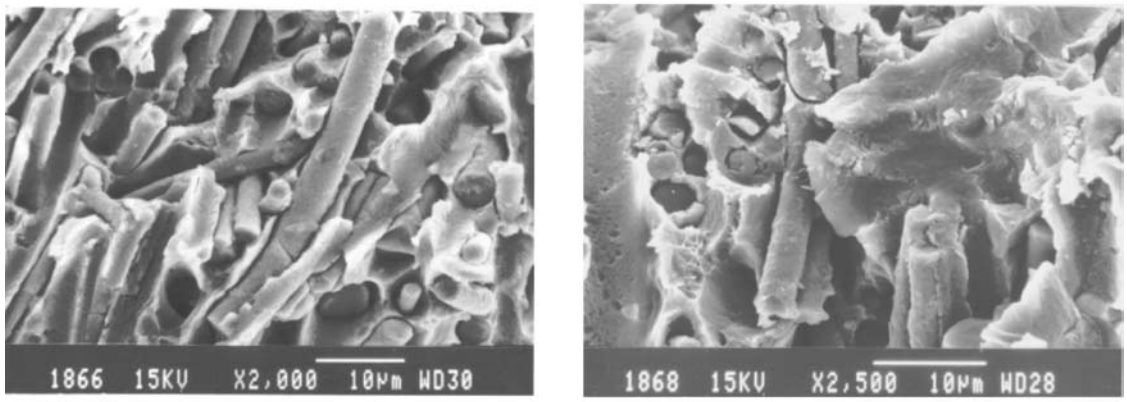

(c) (d)

Figure 7 Fracture surfaces of 20%V_f at (a) room temperature (b & (c) fibre deformation and fibre failure at 100 and 150°C (d) fibre failure due to intense matrix flow at 200°C.

V_{crit} depends largely on the matrix properties such as the ultimate tensile strength and yield strength, and especially on the difference between them (rate of work-hardening), which would affect the plastically induced load transfer to the fibres [27, 31]. In the present case, the value of V_{crit} at room temperature for ZC63 matrix alloy was calculated using equations proposed by Friend [31]. The calculations indicated that a critical volume fraction of >16% is necessary to bring considerable improvement in strength. Hence, in the present case, the behaviour of the composite seems to depend on V_{crit} criteria proposed by Friend [31]. This explains for the lower strength value of 15%V_f composite. It should also be noted that the %elongation of the composite with 15%V_f at room temperature is ~0.5% (Fig. 5b), which is less than the failure strain of short δ-alumina fibres (0.67%) [31]. This further indicates that insufficient fibre content would result at inferior tensile properties. Lower elongation values in Al-and Mg-based

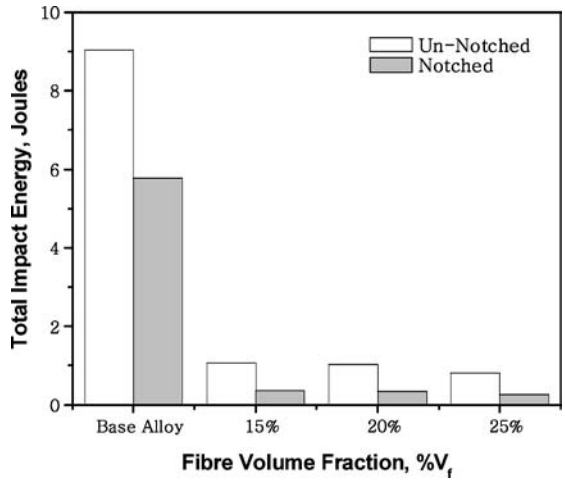

Figure 8 Variation of total impact energy of ZC63 alloy and its composites as a function of fibre volume fraction.

composite systems have also been observed earlier by several authors [22, 27, 31], where the composites exhibited lower strength than that of the unreinforced alloy.

In addition to the critical fibre volume fraction criteria, residual stresses also play an important role in determining the strength of composites at room temperature. Scott and Chen [29] on their work on Al-MMCs, have indicated that the reduction in yield strength in composites when compared to the unreinforced alloy was due to the presence of residual tensile stress in the matrix, which would supplement the externally applied load. Friend [28] had suggested that the magnitude of the residual stresses produced due to the thermal mismatch between the reinforcement and the matrix influenced the strength behaviour of composites at room temperature, and that these stresses would undergo relaxation at higher temperatures. In the present case, the residual stresses were calculated using equations from [33] and were found to be in the range of 75–100 MPa for the composites (15 to 25% V_f) at room temperature. These stresses reduced to < 5 MPa at 200°C. Milliere and Suery [33] had earlier calculated ~65 MPa residual stresses for 15%V_f in Al-MMCs. This indicates that the residual stresses contribute to lowering of strength of composites at room temperature. Fig. 7a shows the fractured surface of 20%V_f composite at room temperature.

With increase in test temperature, relaxation of residual stresses would occur [28]. Further, it should also be noted that the critical fibre volume fraction required to bring about improvement in strength decreases with increase in temperature [28]. For example, in ZC63 matrix alloy, V_{crit} at 100°C > 11%. Hence, owing to these two factors (relaxation of residual stresses and decrease in critical fibre volume fraction, with temperature), the 15%V_f composite shows better strength at higher temperatures.

When compared to that at room temperature, matrix flow at high temperatures occurs due to the ductile nature of the base alloy (Fig. 5b). It has been observed earlier [34] that in the case of ductile matrices, at high temperatures, matrix flow gives rise to mechanical stresses leading to fibre deformation and fibre failure. In the present case, the fractographic studies of the composites tested at 100 and 150°C (Fig. 7b and c) show fibre deformation and fibre failure. From these figures it could also be observed that fibre debonding is less, which could be due to the softening of the Mg $(Zn,Cu)_2$ phase present at the fibre/matrix interface [19] and efficient load transfer to fibres [30] at higher temperatures. With further increase in test temperature to 200°C, intense matrix flow leading to fibre failure is observed (Fig. 7d). This indicates that the transfer of mechanical stresses to fibres intensifies due to increased matrix flow at higher temperatures resulting at lowering of strength. Although the composites exhibit moderate reduction in strength at higher temperatures, their strength remained much greater than that of the unreinforced alloy indicating the positive effect of fibre reinforcement in improving the strength retention characteristics at higher temperatures.

3.4. Impact strength

The total impact energy of unreinforced ZC63 alloy and its composites, for both the un-notched and notched cases,

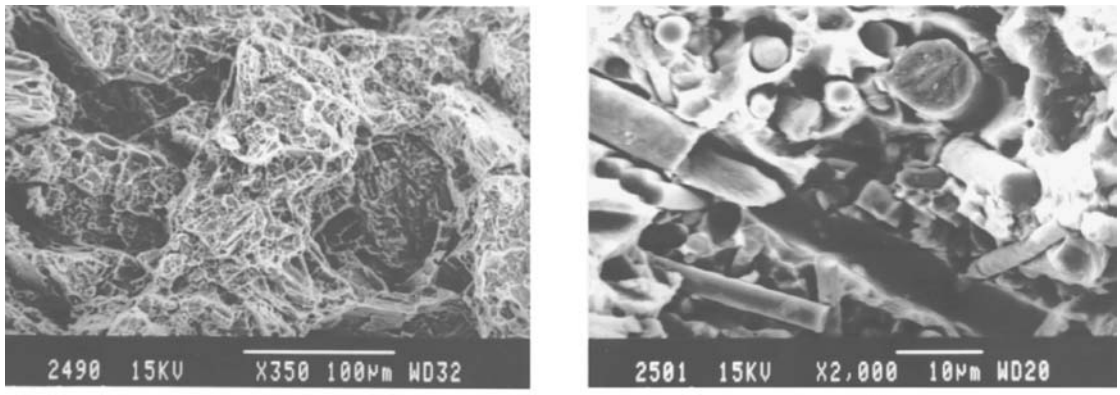

(a) (b)

Figure 9 Fractographic evidences of unreinforced alloy showing (a) prominent ductile failure (un-notched) and (b) 20%V_f composite (un-notched) showing fibre chopping and fibre fracture.

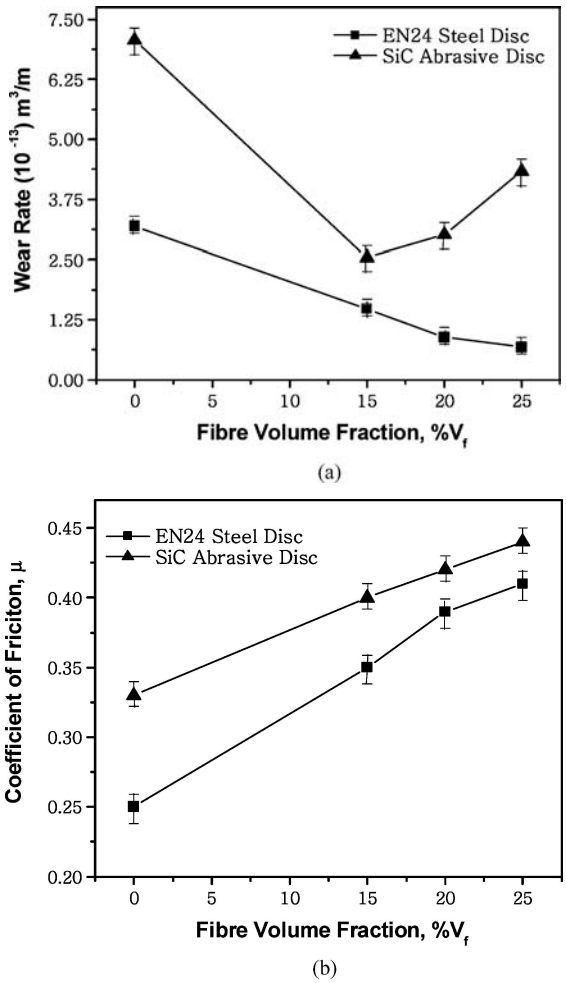

Figure 10 (a) Wear rate of ZC63 alloy and its composites against two different counterfaces and (b) coefficient of friction of ZC63 alloy and its composites against two different counterfaces. (The solid lines are drawn to guide the eye).

are shown in Fig. 8. In both the un-notched and notched conditions, the composites show less resistance to impact loading when compared to the base alloy. This reduction in impact energy with the addition of ceramic reinforcements is due to the inherent brittle nature of the ceramic fibres and also due to the fact that the presence of fibres leads to initiation of cracks at the fibre/matrix interface [35]. Fractographic evidences of the unreinforced alloy in the un-notched condition show prominent ductile fracture (Fig. 9a), which is due to the inherent ductile nature of the unreinforced alloy. Fig. 9b shows a representative fracture surface of 20%V_f composite in the un-notched specimen. In the case of composites, unlike that at the tensile testing conditions where sufficient time is available for the transfer of load from the matrix to the fibres, under impact loading, the time available for load transfer to the fibres is very short, which is due to high strain rates. Thus rapid propagation of cracks occurs under impact loading, leading to matrix fracture, fibre/matrix debonding and fibre fracture resulting in catastrophic failure in the composites [26]. Such observations are evident from Fig. 9b, which reveals fibre chopping and fibre fracture that subsequently led to lowering of the impact strength in the composites. As seen from Fig. 8, the base alloy and the composites in the notched condition absorb less energy in comparison with that of the un-notched. The presence of the notch increases the stress concentration at the tip of the notch and thereby reduces the impact energy [22, 36–38].

3.5. Wear and friction

The wear rates of ZC63 alloy and its composites (slid against two different counterface discs: EN24 Steel and SiC abrasive) are shown in Fig. 10a. For both the alloy and its composites, the wear rate is higher against SiC abrasive disc than against the EN24 steel disc. This is due to the higher hardness and roughness (hardness: ~20 GPa and roughness: ~18.5 μ) of the SiC abrasive media, which results in higher material removal during sliding, when compared to that against the EN24 counterface (hardness –52 HR_c and roughness –0.2μ nm). Against the EN24 counterface, the composites exhibit higher wear resistance than the base alloy. The decrease in wear rate with increase in volume fraction against EN24 counter-

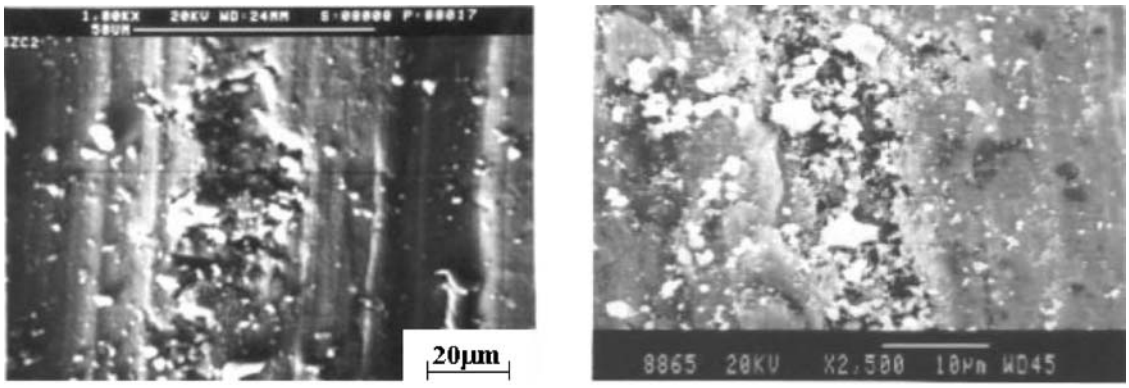

(a) (b)

Figure 11 Worn surface of (a) ZC63 alloy showing adhesion (against SiC counterface) and (b) ZC63 composite (20%V_f) showing delamination (against EN24 counterface).

face (Fig. 10a) is mainly because of the increase in hardness of the composite with fibre volume fraction (Fig. 3). When slid against the SiC counterface, the wear rates of all the composites were lower than that of the unreinforced alloy. However, within the composites the wear rate increases with increase in fibre volume fraction. This further indicates that when slid against SiC counterface, the wear rates of composites do not exhibit any inverse relationship with bulk hardness, as was observed in the case against EN24 disc. Several authors [39, 40] have also observed the absence of the inverse relation between the wear rate and bulk hardness in Al- and Mg-matrix composites. In SiC counterface, the high roughness of the SiC abrasive disc causes trapping of the debris, that are generated during sliding, between the abrasive grits. The debris contains hard ceramic fibres that would act as third body, and subsequently counter-abrade the composite pin material [41]. The counter-abrasion due to the trapped debris intensifies with the increase in the fibre content thereby increasing the wear rate with increase in fibre volume fraction. Fig. 10b shows the variation of coefficient of friction as a function of fibre volume fraction. The composites show higher coefficient of friction when compared to the unreinforced base alloy on both the counterfaces. The presence of hard fibres in the composites acts as the abrasive media to the counterfaces leading to an increase in the friction coefficient [41]. This also explains the increase in coefficient of friction with fibre volume fraction. Fig. 11 (a, b) show the representative worn surfaces of ZC63 alloy (against SiC counterface) and its 20%V_f composite (against EN24 counterface). The unreinforced alloy undergoes material removal by adhesion whereas composites exhibit delamination. In the composites, under repeated sliding, delamination occurs due to the formation of subsurface cracks originating at the fibre/matrix interface. Fig. 11b also shows debris trapped at the delaminated pit due to repeated sliding. Wear due to adhesion in unreinforced alloy and by delamination of the composites have also been reported earlier in AZ91 magnesium alloy and its composites [39, 40].

3.6. Corrosion resistance

Fig. 12 shows the corrosion rate of ZC63 base alloy and its composites as a function of exposure time in salt fog environment. The base alloy exhibits higher corrosion resistance than its composites. For both the alloy and its composites, the corrosion rate increases with time. In the case of composites, corrosion rate also increases with increase in fibre volume fraction, the exception being 25%V_f composite beyond 72 h of exposure.

Fig. 13 shows the corroded surface of ZC63 alloy, which indicates the occurrence of localized corrosion. The corrosion morphology of magnesium alloys depends on the alloy chemistry and environmental conditions [42]. For example, in Mg-Al systems, in which both the cathodic precipitates and the eutectic were present along the grain

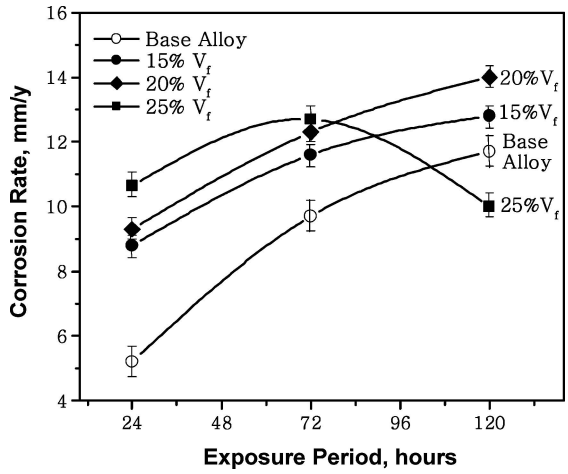

Figure 12 Variation of corrosion rate of ZC63 alloy and its composites on exposure to salt fog environment as a function of exposure time.

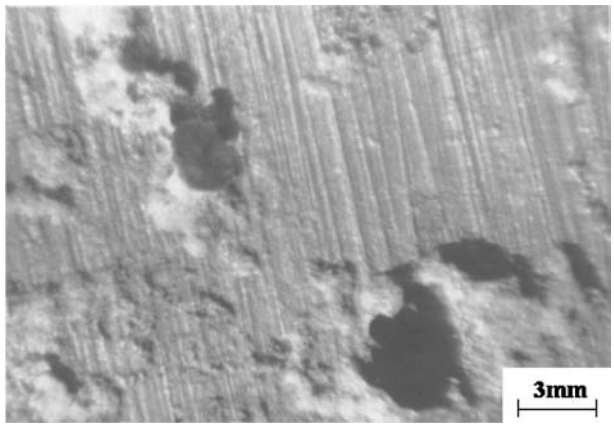

Figure 13 Low magnification micrograph showing localized corrosion of unreinforced ZC63 alloy.

boundaries, uniform corrosion was observed [42, 43], and was explained based on the 'particle undermining model' given by Song *et al.* [41]. The localized corrosion observed in the present case, could be understood in terms of undercutting of the α-magnesium matrix [3, 42–44]. It is well known that, elements or compounds of Cu present in Mg-alloys would act as minute cathodes in the presence of a corrosive medium to the anodic magnesium matrix [45]. These phases would lead to internal galvanic corrosion, which would occur adjacent to the cathode [46]. In the present case, the cathodic Mg $(Zn,Cu)_2$ compound is present along the grain boundaries and the relatively less cathodic $MgZn_2$ precipitates are distributed throughout the matrix [16]. Hence, corrosion would initiate at the highly anodic regions (magnesium matrix), especially at the areas adjoining the grain boundary (cathodic eutectic), as seen in Fig. 14a. It is important to note here that Mg and Mg alloys are virtually immune to inter-granular corrosion attack [43], because of the reason that, in Mg-based alloy systems, the grain boundary phase is invariably cathodic to the Mg- matrix [43, 44]. Hence, the corroded

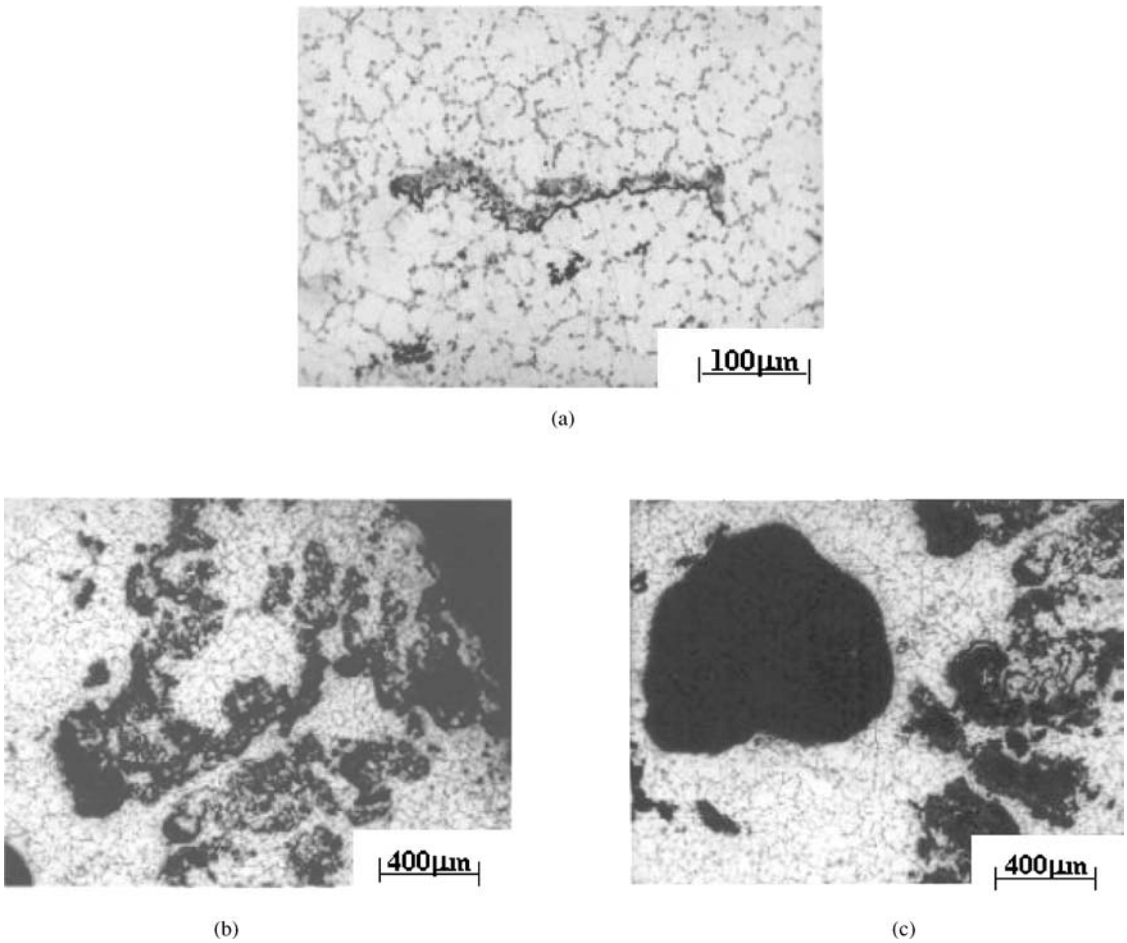

Figure 14 Micrographs showing corroded surfaces of alloy (a) Occurrence of corrosion in regions adjacent to the grain boundary (b & c) further progress of corrosion leading to localized corrosion pit.

region seen in Fig. 12a is not inter-granular; rather it is the region adjacent to the grain boundary. Further, corrosion proceeds simultaneously in many adjoining grains (Fig. 14b) and would eventually undercut the matrix resulting in its falling out. This leaves behind localized pits, as seen in Fig. 14c.

The increase in corrosion rate with increase in fibre volume fraction is due to the increase in the number of cathodic sites with fibre volume fraction [47]. Hence, any addition of reinforcement would cause an increase in the formation of eutectic along the fibre/matrix interface and thereby increase the number of cathodic sites, which makes the magnesium matrix (anode) to increasingly undergo dissolution during corrosion. It is interesting to note that the MMCs with 25%V_f show decrease in corrosion rate at the longest exposure period (Fig. 12). This is believed to result from the initial rapid corrosion that would cause deposition of corroded products on the surface. The deposition of corroded products prevents further exposure of fresh metal surface to the salt fog environment and results in lowering of the corrosion rate. Such retardation of corrosion due to the obstruction of the surface by the corroded products has also been reported earlier by Song *et al*. on Mg-Al-Zn alloys [42].

4. Conclusions

Mg-6Zn-3Cu-0.5Mn alloy (ZC63) and its saffil alumina short fibre reinforced composites were produced using squeeze casting method. The unreinforced alloy and its composites were evaluated for their properties. The major results can be summarized as follows:

(1) Mg-based metal matrix composites produced using squeeze infiltration process provided sound castings with uniform distribution of fibres. The addition of saffil alumina short fibres to the Mg-6Zn-3Cu (ZC63) matrix altered the alloy microstructure and resulted in the substantial improvement in hardness, density and modulus of elasticity.

(2) Although the composites do not show significant improvement in yield strength at room temperature, they exhibited improved strength retention characteristics at temperatures up to 150°C. The properites of the base alloy matrix and the fibre volume fraction play a major role in determining the tensile behaviour.

(3) Composites exhibited low impact strength than the alloy, which is due to the inherent brittle nature of the ceramic fibres.

(4) The wear resistance of the composites showed significant improvement when compared to the unreinforced alloy. The fibre volume fraction and properties of the sliding counterface played a dominant role in determining the wear behaviour.

(5) The composites were relatively less corrosion resistant when compared to their unreinforced counterpart. The corrosion behaviour was strongly dependent on the microstructure of the unreinforced base alloy and the fibre volume fraction.

References

1. N. C. SPARE, *Proc. of London Conference*, Nov 1986, p. 101.
2. A. LUO and M. O. PERQULERYUZ, *J. Mater. Sci.* **29** (1994) 5259.
3. E. F. EMLEY, in "Principles of magnesium technology" (Pergamon Press, London, 1966).
4. W. UNSWORTH, *SAE Tech Paper*, No: 880512 (1989) 2.320.
5. L. DUFFY, *Materials World*, **4** (1996) 127.
6. T. G. NIEH and D. J. CHELLMAN, *Scripta Metall.* **18** (1984) 925.
7. D. F. HASSON, S. M. HOOVER and C. R. CROWE, *J. Mater. Sci.* **20** (1985) 4147.
8. H. FUKUNAGA, S. KOMATSU and Y. KANOH, *Bull. JSME.* **220** (1983) 1814.
9. P. K. BISWAS, S. C. DEV and C. S. S. KRISHNAN, *Indian Foundry J.* **45**(3) (1999) 17.
10. H. HU, *J. Mater. Sci.* **33** (1998) 1579.
11. M. S. YONG and A. J. CLEGG, *Foundryman* (1999) 71.
12. H. WESTENGEN, D. L. ALBRIGHT and A. NYGARD, SAE Tech Paper, No. 900534 (1990) p. 606.
13. Recommended practices for Sand Casting of Aluminium and Magnesium Alloys, 2nd ed. (American Foundryman Society, Des Plaines, IL, 1965).
14. V. VIJAY MOHAN and V. GOPALAKRISHNA, in "Source Book on Magnesium Alloys Tech," (Indian Institute of Metals, Non-Ferrous Metals Division, Bangalore, 1995) p. 1.
15. "Standard practice for Operating Standard Salt Spray (fog) Apparatus," ASTM B117, 1994.
16. C. A. NUNEZ-LOPEZ, P. SKELDON, G. E. THOMPSON, P. LYON, H. KARIMZADEH and T.E. WILKS, *Corrosion Sci.* **37**(5) (1995) 689.
17. W. YANG, G. C. WEATHERLY, D. W. MCCOMB and D. J. LLYOD, *J. Microscopy*, **185** (Pt.2) (1997) 292.
18. Y. Y. KIM, I. S. AHN and T.H. NAM, *Korean J. Mater. Res.* **8**(4) (1998) 362.
19. G. YUAN, H. KATO, K. AMIYA and A. INOUE, *J. Mater. Res.* (Article in Press).
20. Y. KOMURA, M. MITARAI, I. NAKATANI, H. IBA and T. SHIMUZU, *Acta Cryst.* **B26** (1970) 666.
21. LIANG, H. J. SEIFERT, H. L. LUKAS, G. GHOSH, G. EFFENBERG and F. ALDINGER, *Calphad*, **22**(4) (1998) 527.
22. K. PURAZRANG, K. U. KAINER and B. L. MORDIKE,*Composites* **22**(6) (1991) 456.
23. "Composite Materials Handbook," Dept. of Defense, US, Vol. 4, Metal Matrix Composites, 2002.
24. R. J. ARSENAULT and R. M. FISHCHER, *Scripta Metall.* **17** (1983) 67.
25. T. CHRISTMAN and S. SURESH, *Acta Metall.* **36** (1988) 1691.
26. K. K. CHAWLA, in "Metal matrix composites: Structure & Properties of Composites, Materials Science & Technology - A Comprehensive Treatment, 13, 1993 (edited T. W. Chou, V. C. H. Newyork).
27. N. J. MUSSON and T. M. YUE, *Mater. Sci. Eng.* **A135** (1991) 237.
28. C. M. FRIEND, *Scripta Metall.* **23** (1989) 33.
29. V. D. SCOTT and A. S. CHEN, *J. Microscopy*, **196** (1999) 86.
30. H. X. ZHU and S. K. LIU, *Composites* **24** (1993) 437.
31. C. M. FRIEND, *J. Mater. Sci.* **22** (1987) 3005.
32. C. MILLIERE and M. SUERY, *Mater. Sci. Tech.* **4** (1988) 41.
33. S. JAYALAKSHMI, SATISH V. KAILAS, S. SESHAN, *Composites-A*, **33** (2002) 1135.
34. A. G. METCALFE, in "Interfaces in metal matrix composites", Vol 1. edited by L.J. Broutman and Richard H. Brook (Academic Press, New York, 1974) chap. 1.
35. T. LIM, S. Y. LEE and K. S. HAN, *Proc. Amer. Soc. Comp*, 1989, p. 84.
36. S.JAYALAKSHMI, SATISH V. KAILAS, S. SESHAN, *J. Mater. Sci.* **38** (2003) 1383.
37. M. J. DELLIS, J. P. KEUSTERMANS and F. DELANNAY, *Mat. Sci & Eng.* **A135** (1991) 23.
38. GEORGE E. DIETER, in "Mechanical Metallurgy" Metric Edition, (McGraw Hill, 1988) chap. 4.
39. I. M. HUTCHINGS, *Mater. Sci. & Tech.* **10** (1994) 513.
40. A. ALAHELISTEN, F. BERGMAN, M. OLSSON and S. HOGMARK, *Wear* **165** (1993) 221.
41. D. JUN, L. Y. HUI, Y. S. RONG and L. W. FANG, *Wear*, **257** (2004) 930.
42. G. L. SONG and A. ATRENS, *Adv. Eng. Mater.* **1**(1) (1999) 11.
43. G. L. MAKER and J. KRUGER, *Intl. Mater. Rev.* **38**(3) (1993) 138.
44. L. L. SHREIR, in "Corrosion Volume 1" (Newnes - Butterworths, 1965) chap. 4, p. 86.
45. I. J. POLMEAR, in "Light Alloys: Metallurgy of Light Metals" (E. Arnold, Sevenoaks, UK, 1989).
46. A. FROATS, T. K. AUNE, D. HAWKE, W. UNSWORTH and J. HILLIS, in "Metals Handbook," (ASM Intl, 9th Ed, 1987) p. 740.
47. S. L. COLEMAN, V. D. SCOTT and B. MC ENANEY, *J. Mater. Sci.* **29** (1994) 2826.

Received 29 March
and accepted 20 June 2005